Identification of rotor and stator flux linkage maps of squirrel cage induction motors based on identification of rotor time constant maps

Johannes Stoß, Akif Karayel, Leonard Geier, Andreas Liske, Marc Hiller
Karlsruhe Institute of Technology (KIT)
Elektrotechnisches Institut (ETI)
Kaiserstr. 12, Karlsruhe, Germany
E-Mail: johannes.stoss@kit.edu
URL: http://eti.kit.edu

Keywords

«Induction motor», «Flux Model», «Model-based Predictive Control», « Non-linear control».

Abstract

Model-predictive, field-oriented control of squirrel cage induction motors (SCIM) depends on the accurate identification and orientation of rotor and stator flux maps. In this paper, a new method is presented that utilizes the measured rotor time constant maps to reduce the orientation error of the identified flux maps. This enables the identification and modelling of the nonlinear and transient machine behavior, due to the estimation of the stator- and rotor-flux maps in dependence of stator and rotor currents.

1. Introduction

Induction machines are widely used in various applications due to their simple and robust construction as well as low cost [1].
To achieve high-performance control of induction machines, field-oriented control (FOC) is a common technique [2]. It allows decoupling the control of motor torque and flux by transforming the stator currents into a rotating reference frame aligned with the rotor flux space-vector. This requires accurate estimation of the machine flux, which can be obtained by different methods [3–5]. In this paper, a novel identification method for the flux characteristics of induction machines is presented. It enhances existing methods for characterization by an operating point dependent measurement of the rotor time constant. Utilizing the rotor time constant maps, the orientation of the flux maps can be corrected and thus the model and control quality significantly improved.

2. Machine Model

Since the control is performed in rotor flux orientation (RFO), the modelling is based on the rotor flux oriented dq coordinate system as well.
The dq stator voltages ($v_{\mathrm{Sd}}, v_{\mathrm{Sq}}$) are described as a function of the stator resistance R_{s}, the stator dq currents ($i_{\mathrm{Sd}}, i_{\mathrm{Sq}}$), stator flux linkages ($\Psi_{\mathrm{Sd}}, \Psi_{\mathrm{Sq}}$) and the stator angular frequency ω_{s}.

$$v_{\mathrm{Sd}} = R_{\mathrm{s}} \cdot i_{\mathrm{Sd}} + \frac{\mathrm{d}\Psi_{\mathrm{Sd}}}{\mathrm{d}t} - \Psi_{\mathrm{Sq}} \cdot \omega_{\mathrm{s}} \quad (1)$$

$$v_{\mathrm{Sq}} = R_{\mathrm{s}} \cdot i_{\mathrm{Sq}} + \frac{\mathrm{d}\Psi_{\mathrm{Sq}}}{\mathrm{d}t} + \Psi_{\mathrm{Sd}} \cdot \omega_{\mathrm{s}} \quad (2)$$

The rotor voltage equations are given in the same way with the respective rotor quantities. As the rotor is short-circuited, its voltages are $v_{\mathrm{Rd}} = v_{\mathrm{Rq}} = 0$. The rotor flux orientation results in Ψ_{Rq} being zero by definition. Ψ_{Rq} is therefore not included in the equations.

$$v_{\mathrm{Rd}} = 0 = R_{\mathrm{R}} \cdot i_{\mathrm{Rd}} + \frac{\mathrm{d}\Psi_{\mathrm{Rd}}}{\mathrm{d}t} \quad (3)$$

$$v_{\mathrm{Rq}} = 0 = R_{\mathrm{R}} \cdot i_{\mathrm{Rq}} + \Psi_{\mathrm{Rd}} \cdot \omega_{\mathrm{R}} \quad (4)$$

Thereby, the rotor currents, voltages and flux linkages are related to the stator side, allowing a simplified representation of the machine characteristics. To determine the physical rotor quantities, conversion to the rotor side can be performed using the transformers equivalent circuit and the corresponding winding factors [6].

a) Non-linear current model

The following, non-linear modelling for rotor flux and angle estimation is based on [7]. It is known for constant machine parameters as the (linear) current model.
The rotor flux linkages can be defined by the equivalent circuit parameters with L_{m} being the

mutual inductance and $L_{R\sigma}$ as the rotor stray inductance. The rotor q-flux is zero per definition in the rotor flux orientated reference frame.

$$\Psi_{Rd} = L_m \cdot i_{Sd} + (L_{R\sigma} + L_m) \cdot i_{Rd} \quad (5)$$

$$\Psi_{Rq} = 0 = L_m \cdot i_{Sq} + (L_{R\sigma} + L_m) \cdot i_{Rq} \quad (6)$$

It is assumed, that the leakage inductances are constant, since the leakage flux flows primarily through air and cross coupling is not present in the rotor flux oriented reference frame due to $\Psi_{Rq} = 0$. Furthermore, it is assumed that the mutual inductance is affected by saturation and is a function the currents on the d-axis.
The mutual flux linkage is consequently described with L_m being a function of $(i_{Sd} + i_{Rd})$:

$$\Psi_m = (i_{Sd} + i_{Rd}) \cdot L_m(i_{Sd} + i_{Rd}) \quad (7)$$

The rotor angle γ_R which is necessary to calculate the transformation angle γ_S for rotor flux orientated reference frame is determined using the rotor voltage equation (4).

$$\gamma_R = \int \omega_R \, dt = \int -\frac{R_R \cdot i_{Rq}}{\Psi_{Rd}} \, dt \quad (8)$$

The rotor flux is characterized with a first order differential equation based on the assumptions mentioned above and equations (3) and (5):

$$\frac{d\Psi_{Rd}}{dt} = -\frac{R_R}{L_m + L_{R\sigma}}(\Psi_{Rd} - L_m \cdot i_{Sd}) \quad (9)$$

By transferring the linearized equation into the Laplace domain, the transfer behavior is highlighted.

$$\Psi_{Rd} = \frac{L_m \cdot i_{Sd}}{1 + (L_m + L_{R\sigma})/R_R \cdot s} \quad (10)$$

The system has a first order lowpass behavior with the rotor time constant τ_R being defined as:

$$\tau_R = \frac{L_m + L_{R\sigma}}{R_R} = \frac{L_R}{R_R} \quad (11)$$

By transferring the linearized equation (8) into laplace domain and inserting the equation (6), the rotor current dependence is eliminated. Using equations (10) and (11) the block diagram for identification of the rotor angle (fig. 1) can be deduced.
It shows that the rotor angle γ_R for the rotor flux orientation thereby only depends on the dq-currents and the correct value of the rotor time constant, which is further analyzed and identified in this paper.

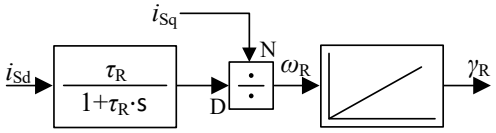

Fig. 1.: Estimation of the rotor angle γ_R using the nonlinear current model.

The transformation angle γ_S for the rotor flux orientated reference frame is determined with the use of the mechanical angle γ_M from the angle encoder multiplied by the number of pole pairs p.

$$\gamma_S = \gamma_R + \gamma_M \cdot p \quad (12)$$

The power balance can then be used to determine the inner torque T_e [5].

$$T_e = \frac{3p}{2}\left(\Psi_{Sd} i_{Sq} - \Psi_{Sq} i_{Sd}\right) \quad (13)$$

$$T_e = -\frac{3p}{2}\Psi_{Rd} i_{Rq} \quad (14)$$

This calculation is made under neglection of iron losses.

3. Standard identification scheme

This section describes the first part of the identification procedure. It is assumed that only the number of pole pairs is known from the machine. To carry out the identification, a load machine and a power converter with output current and voltage measurements are required. The rotor position must be known as well.

a) Basic machine parameters

First, the linear mutual and leakage inductance as well as the rotor and stator resistance are identified.
The ohmic voltage drop of the individual lines is determined at standstill using an impressed dc stator current. This process is also repeated periodically later during the measurement routines to compensate for a temperature rise in the machine and thus a change in the stator resistance.
The linear mutual and leakage inductances together with the rotor time constant are determined via locked rotor and no load tests [8]. This data is then used to set up a controller for the FOC [7].

b) Flux maps in arbitrary orientation

Usually, the machine flux identification is carried out by means of a current or voltage model using the constant parameters identified in 3 a). Since the machine parameters change, for example due to saturation and current displacement, this inevitably leads to misorientation.
As a result, the fluxes determined in this section are not aligned to the rotor flux-oriented reference frame, but to an arbitrary reference frame, which is defined by the identified linear machine parameters. Therefore, the displacement from the rotor flux-oriented system depends on the current operating point. Detailed investigation into detuning of the current model and its effects is also shown in [9].
In contrast to previous methods [4, 5], the identification is not performed at a constant speed but at a constant stator angular frequency using the FOC as proposed in [3]. This is based on the assumption that iron losses occur primarily in the stator and depend on both stator frequency and amplitude [10]. By measuring at a constant stator angular frequency, the frequency dependence can be eliminated and thus the accuracy is improved.
The measuring range must be restricted accordingly, as operating points with large rotor frequency lead to high mechanical speeds n_m. For steady state operating points, as present in the identification, the d-rotor current is completely decayed. Using equations (8) and (10) under the assumption of constant currents, the rotor angular frequency can be estimated by applying the final value theorem $\lim_{t\to\infty} f(t) = \lim_{s\to 0} s \cdot F(s)$ on the step response $F(s) = \frac{1}{s} \cdot G(s)$ of the transfer function $G(s)$:

$$\omega_\mathrm{R} = \lim_{s\to 0} \frac{i_\mathrm{Sq}}{\left(\frac{\tau_\mathrm{R}}{1+\tau_\mathrm{R}\cdot \mathrm{s}}\right)\cdot i_\mathrm{Sd}} = \frac{i_\mathrm{Sq}}{\tau_\mathrm{R}\cdot i_\mathrm{Sd}} \tag{15}$$

Therefore, the mechanical rotor speed is dependent on the driven operating point by:

$$n_\mathrm{m} = \frac{60\,\frac{\mathrm{s}}{\mathrm{min}}}{2\pi\cdot p}\left(\omega_\mathrm{S} - \frac{i_\mathrm{Sq}}{\tau_\mathrm{R}\cdot i_\mathrm{Sd}}\right) \tag{16}$$

For setpoints with zero or almost zero stator d-current the required mechanical speed tends to negative or positive infinity. For this reason, those setpoints are omitted from the measurements which can be seen in fig. 2. The distribution of the setpoints is done in polar coordinates to maintain the current limit of the machine. The evaluation of the measurement is performed by solving equations (1) and (2) for the flux linkage.

$$\Psi_\mathrm{Sd} = \frac{v_\mathrm{Sq} - R_\mathrm{s}\cdot i_\mathrm{Sq}}{\omega_\mathrm{S}} \tag{17}$$

$$\Psi_\mathrm{Sq} = \frac{-v_\mathrm{Sd} + R_\mathrm{s}\cdot i_\mathrm{Sd}}{\omega_\mathrm{S}} \tag{18}$$

In steady state operation the flux linkages are constant and thus their time derivative becomes zero.
To precisely determine the fundamental flux linkage, the average value is taken over several mechanical periods. This ensures that manufacturing tolerances and thus harmonics with low mechanical orders have no impact on the result. To compensate the voltage drop across the stator resistance, it is periodically measured as described in section 3 a). The procedure of 3 b) is also described in detail for constant rotational speeds in other publications [3–5].

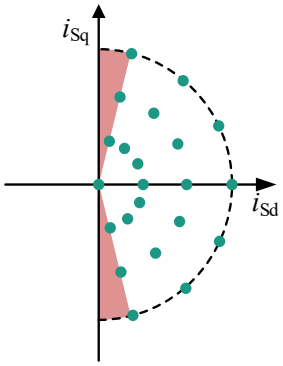

Fig. 2.: Setpoints and non-measurable area due to high mechanical speeds.

4. Reorientation of the flux maps

To eliminate the misorientation of the flux maps identified in 3 b) a novel procedure is presented in the following chapter. For that, the rotor time constant is identified for the entire operating area. This leads to significantly increased model and control quality due to improved orientation.

a) Rotor time constant identification using stationary measurements

This section describes the identification of the rotor time constants based on the known measurement data. Subsequently, a transient measurement routine is presented.
Using the stationary measurement data of 3 b) the rotor time constant can be determined

retrospectively without performing additional transient measurements. In steady-state operation, it is derived from equation (3) that the rotor d-current completely decays. As the stator q-flux in RFO is the stray flux, the amplitude of the flux linkage is primarily built up via the stator d-current. The required d-current for the measured flux amplitude $\hat{\Psi}_S$ is estimated using the no-load characteristic. This requires the q-flux linkage and cross coupling to be small compared to the d-flux linkage. The mapping of the no load characteristics of 3 a)

$$\Psi_{Sd,no\,load}: i_{Sd} \rightarrow \hat{\Psi}_S \tag{19}$$

is therefore transformed into the inverse mapping to identify i_{Sd}.

$$\Psi^{-1}_{Sd,no\,load}: \hat{\Psi}_S \rightarrow i_{Sd} \tag{20}$$

Based on the measured current amplitude, the q-current can be calculated subsequently. The rotor time constant is then determined for each setpoint using equation (15).

$$\tau_R = \frac{i_{Sq}}{\omega_R \cdot i_{Sd}} = \frac{i_{Sq}}{\left(\omega_S - n_m \frac{2\pi p}{60 \frac{s}{min}}\right) \cdot i_{Sd}} \tag{21}$$

This allows the estimation of the rotor time constant using only the recorded rotor angular frequency and the dq currents of the conducted routine in 3 b). Since a division by zero is not defined, this method does not allow parameter identification at no-load condition.

b) Rotor time constant identification using transient measurements

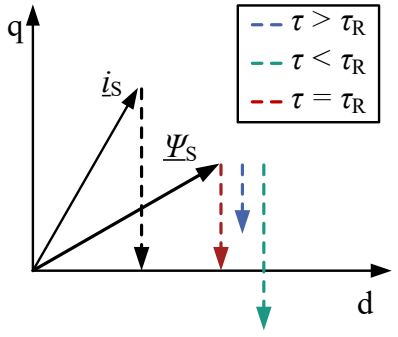

Fig. 3.: Basic principle of the rotor time constant measurement.

Due to the rotor dynamics of the induction machine, the rotor flux orientation can also be determined by evaluating the transient behavior. This requires, the rotor dynamics to be significantly smaller than the achievable dynamics of the current control in the stator circuit. The procedure is related to [11]. For the transient rotor time constant measurement, the stationary operating point is approached first. Afterwards, the q-current is set to 0 A while the d-current setpoint remains unchanged (black dotted arrow in fig. 3).

With ideal orientation (fig. 3&4 red) the stator q-flux should fall with the dynamics achieved by the current control strategy to 0 Vs since the q-flux is only a leakage flux fed by the stator q-current. If the rotor time constant is too small or too large, a misorientation occurs. It leads to a portion of the relatively slow changing d-flux being falsly assigned to the q-axis. This can be seen by the decay of the q-flux with the rotor time constant in the misoriented system (fig. 3&4 green, blue).

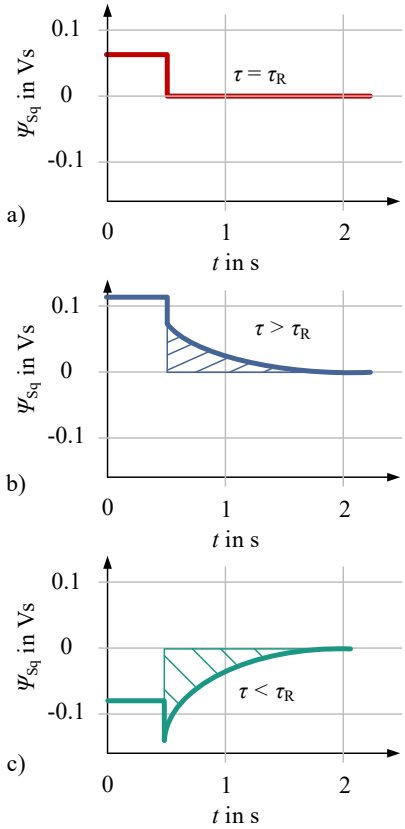

Fig. 4.: Basic principle of the rotor time constant measurement.

The flux linkages are estimated using the voltage equations (17) and (18). By evaluating the error integral ($e = \int \Psi_{Sq} dt$) over time (Fig. 4), it can be directly deduced whether the value for the rotor time constant τ is larger or smaller than the real value τ_R.

The procedure is initiated with two random time constants in the expected range. Using linear interpolation between two measurements (Fig. 5), an improved rotor time constant is calculated and subsequently identified.

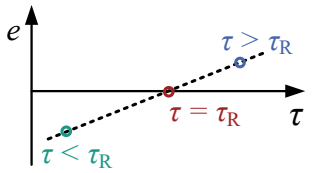

Fig. 5.: Linear approximation of the rotor time constant.

The procedure is repeated using the two rotor time constants with the smallest error integral until the identification error is sufficiently small or the maximum number of measurement cycles is exceeded.

c) Reorientation of flux maps

In the final step, the correct current space vector is calculated for each flux point from 3 b). The system is therefore transformed into polar representation, describing each measurement point by its angle and current amplitude ($\hat{\imath}, \gamma_{\mathrm{CV}}$) or flux amplitude ($\hat{\Psi}, \gamma_{\mathrm{CV}} + \gamma_{\Delta\Psi\mathrm{i}}$) in rotor flux orientation. Thereby the angle $\gamma_{\Delta\Psi\mathrm{i}}$ denotes the angle between flux and current vectors determined in the arbitrary orientation in 2 b).
The measurements in 3 b) allow determination of the stator flux amplitudes $\hat{\Psi}$ and current amplitudes $\hat{\imath}$ as well as their relative orientation by $\gamma_{\Delta\Psi\mathrm{i}}$, but not the precise alignment in rotor flux orientation. Consequently, calculation of the angle γ_{CV} is required. It is defined in an accurately aligned system as:

$$\gamma_{\mathrm{CV}} = \tan^{-1}\left(\frac{i_{\mathrm{Sq,co}}}{i_{\mathrm{Sd,co}}}\right) \tag{22}$$

As the orientation of the correct aligned currents $i_{\mathrm{Sd,co}}$ and $i_{\mathrm{Sq,co}}$is not known, equation (22) is transformed using (15). Resulting in an equation only dependent on measured parameters:

$$\gamma_{\mathrm{CV}} = \tan^{-1}\left(\frac{1}{\omega_{\mathrm{R}} \cdot \tau_{\mathrm{R}}}\right) \tag{23}$$

Reorientation is performed via the measured rotor time constants from 4 a) or 4 b). The rotor angular velocity is determined as before by the stator angular frequency and the measured rotational speed.

The currents ($i_{\mathrm{Sd,co}}, i_{\mathrm{Sq,co}}$) are subsequently transformed back into the cartesian coordinate system with their corrected orientation using γ_{CV}.

$$i_{\mathrm{Sd,co}} = \hat{\imath} \cdot \cos\left(\gamma_{\mathrm{CV}}\right) \tag{24}$$

$$i_{\mathrm{Sq,co}} = \hat{\imath} \cdot \sin\left(\gamma_{\mathrm{CV}}\right) \tag{25}$$

The same transformation is applied to the flux linkages using the additional angle between current and flux linkage $\gamma_{\Delta\Psi\mathrm{i}}$:

$$\Psi_{\mathrm{Sd,co}} = \hat{\Psi} \cdot \cos\left(\gamma_{\mathrm{CV}} + \gamma_{\Delta\Psi\mathrm{i}}\right) \tag{26}$$

$$\Psi_{\mathrm{Sq,co}} = \hat{\Psi} \cdot \sin\left(\gamma_{\mathrm{CV}} + \gamma_{\Delta\Psi\mathrm{i}}\right) \tag{27}$$

d) Estimation of the rotor flux map

Since the rotor current and rotor flux cannot be measured in the SCIM, the rotor map can only be estimated indirectly. In [5], the identification is carried out via torque measurement. It is therefore assumed that the rotor resistance can be determined in advance and all torque components that arise, for example, due to friction and iron losses, can be compensated. Since the precise determination of these proportions is very time-consuming, a different approach is used in this paper.

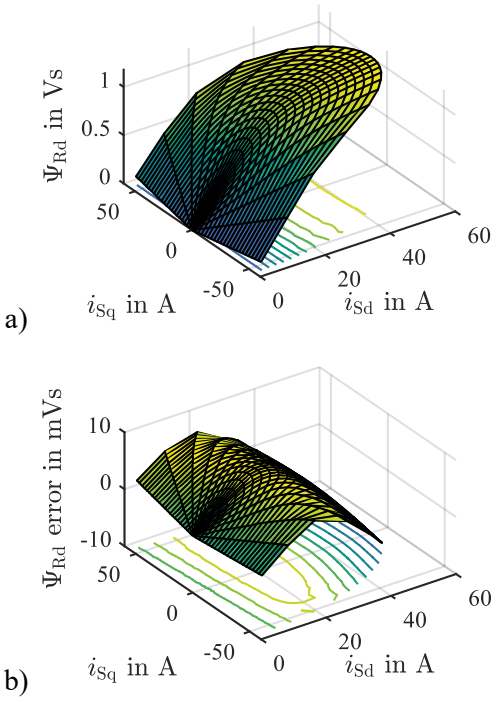

Fig. 6.: a) FEA simulation of stator d flux linkage and b) error of rotor flux estimation.

The rotor flux is estimated using the identified flux linkage map and the leakage inductance. It is therefore assumed that the leakage flux is primarily outside the iron and thus is hardly influenced by saturation. The leakage inductance is thus assumed to be constant. Fig. 6 shows the rotor flux linkage and the error of the predicted rotor flux linkage of a SCIM from a finite element analysis (FEA) simulation. Since no precise data is available for the device under test (DUT) described in chapter 6, the FEA model was taken from [12] and scaled accordingly.
As expected, the error of the estimated rotor flux linkage based on a constant leakage inductance is below 2 % even when the d-flux linkage saturates. It can therefore be assumed that the model error using this estimation is relatively small.
Compared to methods that rely on torque and loss modelling the model error is generally assumed to be equal or lower due to the shorter measurement chain and reduced dependency of machine parameters like temperature and speed.

e) Estimation of dynamic flux maps

The modeling and identification shown so far covers the steady-state behavior of the machine. To represent dynamic characteristics, the maps must be extended by the dimension of the d rotor current i_{Rd}. This is necessary as the assumptions of the steady-state condition $i_{\mathrm{Rd}} = 0$ is no longer valid for dynamic operations. Driven by the fact, that saturation is almost exclusively present on the mutual inductance and can be neglected for the stray inductances, the flux linkages can be estimated for $i_{\mathrm{Rd}} \neq 0$. Therefore, the mutual inductance is modeled in dependence of the magnetomotive force and therefore the currents as shown in equation (7).
The current through the mutual inductance, which leads to the mutual flux linkage, corresponds to the magnetizing current, which is defined as [7]:

$$i_{\mu} = i_{\mathrm{Sd}} + i_{\mathrm{Rd}} \tag{28}$$

To take cross saturation into account, the mutual flux is determined from the identified stationary flux maps in 3 c) assuming $i_{\mathrm{Rd}} = 0$ and $i_{\mu} = i_{\mathrm{Sd}}$:

$$\Psi_{\mathrm{m}} = \Psi_{\mathrm{Sd}}(i_{\mu}, i_{\mathrm{Sq}}) - L_{S\sigma} \cdot i_{\mathrm{Sd}} \tag{29}$$

Using the magnetizing current, the mutual flux linkage can now also be described as a function of the rotor current.
This leads to the following expression for the stator and rotor flux linkages:

$$\Psi_{\mathrm{Sd}} = \Psi_{\mathrm{m}}(i_{\mathrm{Sd}} + i_{\mathrm{Rd}}, i_{\mathrm{Sq}}) + L_{\mathrm{S}\sigma} \cdot i_{\mathrm{Sd}} \tag{30}$$

$$\Psi_{\mathrm{Sq}} = \Psi_{\mathrm{Sq}}(i_{\mathrm{Sd}} + i_{\mathrm{Rd}}, i_{\mathrm{Sq}}) \tag{31}$$

$$\Psi_{\mathrm{Rd}} = \Psi_{\mathrm{m}}(i_{\mathrm{Sd}} + i_{\mathrm{Rd}}, i_{\mathrm{Sq}}) + L_{\mathrm{R}\sigma} \cdot i_{\mathrm{Rd}} \tag{32}$$

Based on the FEA simulation in 3 d), the relative average error in the dynamic model can also be evaluated. It is assumed that the leakage inductances are evenly distributed on the stator and rotor side, since an exact distribution cannot be determined later by measurement and thus also leads to a modeling error. The error determined by this method is less than 0.9% with regard to the respective maximum value of the flux component. Thus, a sufficient correlation of the model is to be expected.

5. Testbench

The DUT is a *Siemens 1LE1592-1EB42-1AF4* SCIM. The same machine is used as load (fig. 7). The characteristics according to the datasheet are given in table I. The DUT features a sensor for stator temperature monitoring. Rotor temperature sensing is not provided.

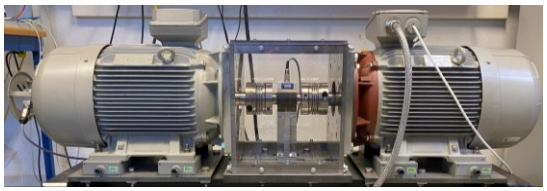

Fig. 7.: Testbench of the *Siemens 1LE1592-1EB42-1AF4.*

Signal processing and control is performed on the *ETI-SoC system*, which is based on the *Xilinx Zynq 7030* [13]. To allow a fast adaptation of the software to different test scenarios, the code generation is performed using *MATLAB® Simulink Code generation*.
The test bench runs at a switching and controller frequency of 10 kHz. The DUT and load are powered by the two-level IGBT *ETI-EPSR* shown in [13]. It provides the *LEM LA 100-P* sensors for current measurement with an accuracy of 0.5 % as well as the line voltage measurement with approx. 2 % accuracy.
The signals are recorded by a *Texas Instruments THS1206* 12-bit AD converter with 1.5 MSPS per channel and averaged for each switching period. The rotor angle is measured via a 10-bit

incremental encoder, which is operated with 4-fold evaluation. This results in 12-bit resolution.

Table I: Linear characteristics of the DUT [14]

Symbol	Meaning	Value
P_N	Nominal power	22 kW
m	Total weight	170 kg
V_N	Nominal voltage	380 V
I_N	Nominal current	45 A
n_N	Nominal speed	1500 rpm
p	Pole pairs	2
R_S	Stator resistance	154 mΩ
R_R	Transformed rotor resistance	103 mΩ
$L_{s\sigma}$	Stator stray inductance	2.5 mH
$L_{R\sigma}$	Transformed rotor stray inductance	0.93 mH
L_m	Mutual inductance	35.82 mH
τ_R	Rotor time constant	0.35 s

6. Measurement Results

In this section, the measurement results from the test bench presented in chapter 5 are shown. The data was not smoothed or filtered in any kind. The measurements from 3 a) are not explicitly shown, as they are only used to configure the FOC.
This section focuses on the operation principle of the identification. Therefore, the measurements of the flux linkages are only carried out at one stator frequency which corresponds to about half the nominal frequency to reduce the impact of iron losses. This is also a common technique for PMSM parameter identification [15].
To improve the accuracy of control methods and machine models for the entire speed range the same routine can be carried out at different stator frequencies. This allows the flux linkages to be additionally modelled in dependence of stator frequency.

a) Flux maps in arbitrary orientation

Since the results from 3 b) differ from previous methods due to the measurement at constant stator angular frequency, the results are shown here in detail. The measurement is conducted at a constant stator frequency of 25 Hz. The current amplitude is varied between 0 A and 55 A in 2.5 A steps. The current angle is limited according to (15) varied in the range of -88° to 88° in 8° steps. This results in 529 operating points. The rotor time constant of the current model is set to 0.24 s as identified by the measurements described in 3 a).

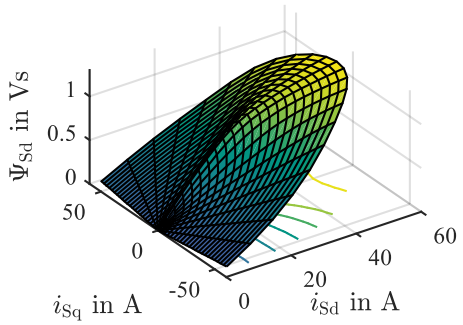

Fig. 8.: d-flux linkage in arbitrary orientation

In each operating point, measurement data of 25 mechanical periods are recorded. These are averaged afterwards for evaluation. Furthermore, a DC measurement is conducted periodically to track the stator resistance. Temperature control of the machine is not technically possible, so deviations in the parameters may occur due to temperature changes within the machine. Due to the low power density of 0.13 $^{kW}/_{kg}$, these are assumed to be small.
Fig. 8 shows the d-flux linkage. The saturation of the machine can be clearly observed. The decrease in the curve towards larger q-currents indicates cross-coupling. As will be shown in the next chapter, the strong cross-coupling of the d-flux linkage is an artifact caused by the misorientation of the coordinate system.

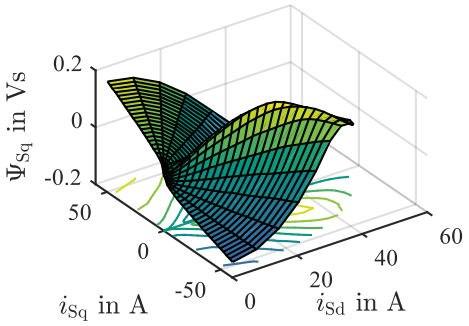

Fig. 9.: q-flux linkage in arbitrary orientation.

The q-flux linkage in fig. 9 shows obvious misorientation error. Since the error changes in dependence of the setpoint, no physically reasonable interpretation is possible.

b) Rotor time constant

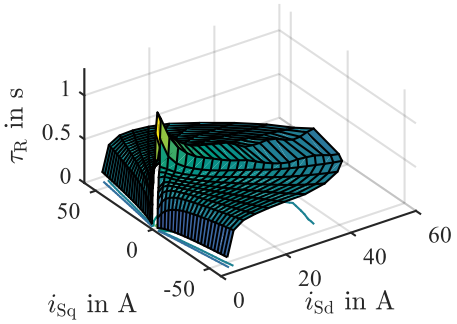

Fig. 10.: Estimated rotor time constant based on the stationary measurements.

To improve the orientation of the coordinate system, the procedures for determining the rotor time constants from 4 a) are now applied. First, the rotor time constant map is calculated based on the stationary measurements. The results are shown in fig. 10. A significant dependence on the operating point can be seen here. It is also clear that a control and evaluation with a constant rotor time constant of 0.24 s leads to a clear misorientation of the coordinate system as indicated in the previous chapter.

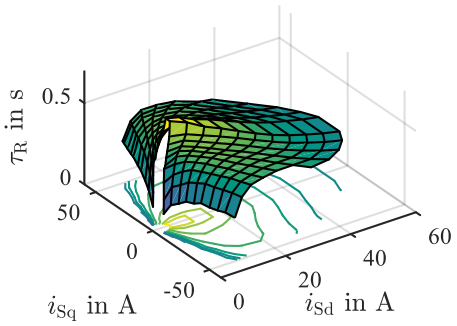

Fig. 11.: Measured rotor time constant based on transient measurements.

Fig. 11 shows the map of the rotor time constant identified by the transient measurements. Since the measurement is significantly more time-consuming than the steady-state characterization, only 242 operating points were evaluated.
Due to the symmetry to the q-axis, the results are subsequently averaged between motor and generator operating points.
Compared to the map determined in fig. 10, the transient measured values of the rotor time constant are slightly lower. The deviation is mostly below 0.1s. The peak of the time constant is also absent in the transient measurement at low current amplitudes in fig. 11, which provides a better representation of the real machine behavior. The deviation in the stationary determination can be explained by the approximations used to estimate the d-flux linkage in (19).

c) Reorientated flux maps

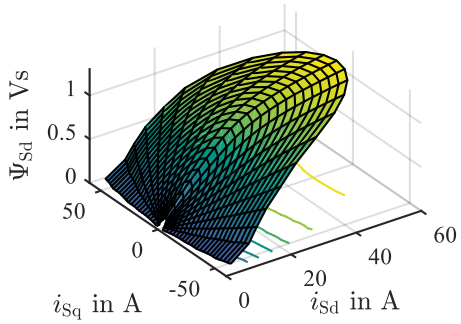

Fig. 12.: d-flux linkage in rotor flux orientation using transient measurements.

Based on the transient measured rotor time constants, the orientation of the flux maps are corrected below. The modified d-flux linkage shows a clearly changed shape.
Saturation is also clearly recognizable here, but in comparison to the arbitrary orientation, the cross-coupling is significantly reduced by the improved alignment.
For q-flux linkage, the changed location of the current setpoints results in a different shape of the curve. In comparison to the arbitrary orientation, the reoriented q-flux map matches the general model description whereby the q-flux is formed only by the leakage inductances. Thus, the amplitude in fig. 13 is small compared to the d-flux linkage and no saturation occurs.

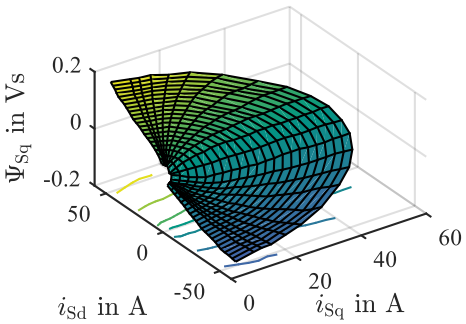

Fig. 13.: q-flux linkage in rotor flux orientation using transient measurements.

Fig. 14 shows the rotor flux linkage. The shape of the rotor flux linkage is similar to the stator d-flux linkage. The total leakage inductance was determined in advance to 2.47 mH by the locked rotor test. It is assumed that it is equally

distributed between the stator and rotor leakage inductance. Alternatively, a distribution based on the ratios given in the data sheet or an estimation of the distribution according to [16] can be applied.

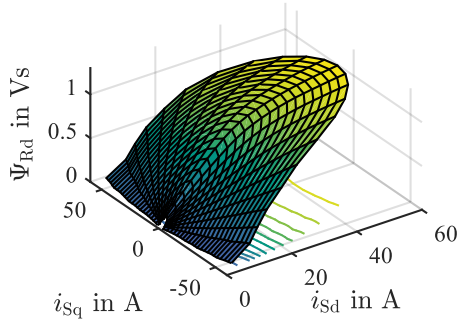

Fig. 14.: Rotor flux linkage in rotor flux orientation

d) Dynamic flux maps

Based on the previously determined steady-state flux maps, the dynamic maps are now computed using the calculations in 3 d). For illustration reasons, only the maps for constant rotor d-currents of ±10 A are now shown as examples.

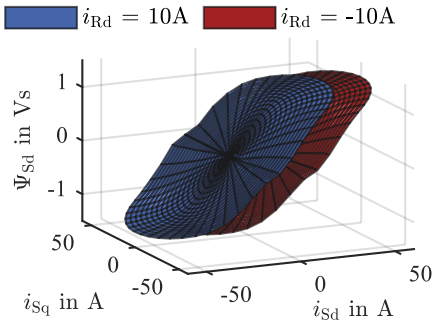

Fig. 15.: Stator d-flux linkage in rotor flux orientation at $i_{Rd} = \pm 10$ A

To allow modelling for negative d-currents, the maps are first expanded by utilizing their symmetry. Further extension of the maps for use in machine models or control algorithms, can be achieved by fitting and extrapolating the flux linkage maps. As this must be carried out individually for each system, only the measured data without extrapolation is shown here.

A slight discontinuity is visible in the area of small d-currents and large q-currents. This is the high rotor frequency and the small rotor flux linkages in this area, causing the measurements to have higher risk of error.

Since the induction motor is simplified modelled as a system with three different windings (Sd, Sq, R) in rotor flux orientation, the rotor current dependent evaluation shows a comparable behavior to flux maps of Electrically Excited Synchronous Machines (EESM) [17].

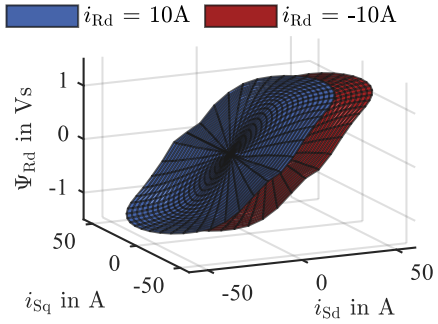

Fig. 16.: Rotor flux linkage in rotor flux orientation at $i_{Rd} = \pm 10$ A

As expected, positive rotor d-currents lead to an increased amplitude of the mutual flux. This is also clearly visible in the rotor d-flux linkage and the stator d-flux linkage (fig. 15 and fig. 16). Thereby, the rotor d-flux linkage differs slightly from the stator d-flux linkage due to the stray flux as already observed in 6 c).

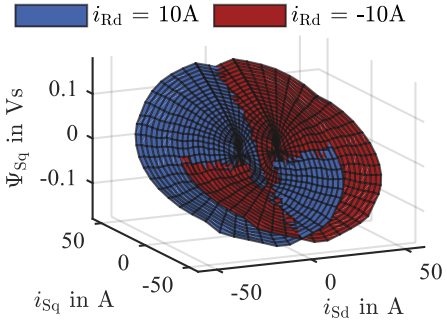

Fig. 17.: Stator q-flux linkage in rotor flux orientation at $i_{Rd} = \pm 10$ A

A slight cross saturation can be recognized at the q-flux linkage due to the visualization of different rotor currents. Compared to the EESM it is less pronounced due to the rotor flux orientation.

7. Conclusion and Outlook

In this paper, methods for the determination of rotor time constant as a function of the operating point were introduced. Based on these results, a procedure for the subsequent correction of the orientation of measured flux linkage maps was presented.

To take dynamic operation into account, those maps were extended analytically to the dimension of the rotor current. All results are based on non-linear modelling of the induction motor.

Including a novel non-linear current model for rotor flux- and angle estimation. Those lead to a significant improvement of the orientation and thus of the model accuracy for the field-oriented control. Furthermore, the map of the rotor flux linkage can be determined based on the measured data.

All results presented in this paper were generated by measurements on the test bench in order to demonstrate the feasibility under real operating conditions. The measurement results were not smoothed or filtered in order to allow a unbiased evaluation of the results.

As it was not possible to record the rotor temperature directly in this test setup, the influence of the rotor temperature on the measurement result cannot be determined precisely. Future tests should therefore include rotor telemetry to enable appropriate rotor temperature control and monitoring. As the thermal time constant of the DUT is large compared to the measurement duration and the DUT was in thermal balance at the beginning of the measurement routine, no significant deviations from the presented results are to be expected.

8. References

[1] Z. Q. Zhu and D. Howe, "Electrical Machines and Drives for Electric, Hybrid, and Fuel Cell Vehicles," *Proc. IEEE*, vol. 95, no. 4, pp. 746–765, 2007, doi: 10.1109/JPROC.2006.892482.

[2] P. C. Sen, "Electric motor drives and control-past, present, and future," *IEEE Trans. Ind. Electron.*, vol. 37, no. 6, pp. 562–575, 1990, doi: 10.1109/41.103462.

[3] J. Kullick and C. M. Hackl, "Nonlinear Modeling, Identification, and Optimal Feedforward Torque Control of Induction Machines Using Steady-State Machine Maps," *IEEE Trans. Ind. Electron.*, vol. 70, no. 1, pp. 211–221, 2023, doi: 10.1109/TIE.2022.3153811.

[4] L. Tolosano, E. Armando, S. Rubino, F. Mandrile, and R. Bojoi, "Experimental Identification of Induction Machine Flux Maps for Traction Applications," in *2022 IEEE Energy Conversion Congress and Exposition (ECCE)*, Detroit, MI, USA, Oct. 2022 - Oct. 2022, pp. 1–8.

[5] J. Kullick and C. M. Hackl, "Generic machine identification and maximum efficiency operation of induction machines," Dec. 2018. [Online]. Available: https://arxiv.org/pdf/1812.02431

[6] A. Binder, *Elektrische Maschinen und Antriebe: Grundlagen, Betriebsverhalten,* 2nd ed. Berlin, Heidelberg: Springer Berlin Heidelberg, 2018. [Online]. Available: http://nbn-resolving.org/urn:nbn:de:bsz:31-epflicht-1506482

[7] Felix Blaschke, "Das Verfahren der Feldorientierung zur Regelung der Drehfeldmaschine," (in German), 1973. [Online]. Available: https://research.tue.nl/en/publications/das-verfahren-der-feldorientierung-zur-regelung-der-drehfeldmasch

[8] *IEEE Standard Test Procedure for Polyphase Induction Motors and Generators: IEEE Standard 112-2017 Revis. IEEE Standard 112-2004*, Piscataway, NJ, USA, Feb. 2018.

[9] W. Zägelein, "Drehzahlregelung des Asynchronmotors unter Verwendung eines Beobachters mit geringer Parameterempfindlichkeit," Diss. Uitgever niet vastgesteld, 1984.

[10] E. Levi, M. Sokola, A. Boglietti, and M. Pastorelli, "Iron loss in rotor-flux-oriented induction machines: identification, assessment of detuning, and compensation," *IEEE Trans. Power Electron.*, vol. 11, no. 5, pp. 698–709, 1996, doi: 10.1109/63.535402.

[11] L. Niu, X. Liu, Y. Wang, A. K. Gupta, and J. Zhai, "Induction machine rotor time constant identification using bisection search method," in *Proceedings of the 2016 IEEE Region 10 Conference (TENCON): November 22-25, 2016, Marina Bay Sands, Singapore*, Singapore, 2016, pp. 3648–3652.

[12] *InductionMotorExample:Finite Element Method Magnetics.* [Online]. Available: https://www.femm.info/wiki/InductionMotorExample (accessed: Mar. 24 2023).

[13] R. Schwendemann, S. Decker, M. Hiller, and M. Braun, "A Modular Converter- and Signal-Processing-Platform for Academic Research in the Field of Power Electronics,"

in *2018 International Power Electronics Conference (IPEC-Niigata 2018 -ECCE Asia)*, 2018, pp. 3074–3080.

[14] Siemens AG, *Datasheet: Siemens 1LE1592-1EB42-1AF4.* [Online]. Available: https://mall.industry.siemens.com/mall/de/DE/Catalog/Product/teddatasheet/?format=PDF&caller=Mall&mlfbs=1LE1592-1EB42-1AF4%20%20&language=de (accessed: Jun. 29 2023).

[15] S. L. Kellner, M. Seilmeier, and B. Piepenbreier, "Impact of iron losses on parameter identification of permanent magnet synchronous machines," in *2011 1st International Electric Drives Production Conference (EDPC 2011): Nuremberg, Germany, 28 - 29 September 2011*, Nuremberg, Germany, 2011, pp. 11–16.

[16] D. Schröder, *Elektrische Antriebe - Regelung Von Antriebssystemen,* 4th ed. Berlin, Heidelberg: Springer Berlin / Heidelberg, 2015. [Online]. Available: https://ebookcentral.proquest.com/lib/kxp/detail.action?docID=4182222

[17] P. Winzer, J. Richter, and M. Doppelbauer, "Dynamic control of generalized electrically excited synchronous machines using predictive flux control," in *Dynamic Control of Generalized Electrically Excited Synchronous Machines Using Predictive Flux Control*, Florence, Italy, 2016, pp. 2772–2777.